Bioactive Materials 31 (2024) 136–150

Contents lists available at ScienceDirect

Bioactive Materials

journal homepage: www.keaipublishing.com/en/journals/bioactive-materials

Modeling human brain rhabdoid tumor by inactivating tumor suppressor genes in induced pluripotent stem cells

Timothy Hua [a,2,1], Yu Xue [a,1], Drishty B. Sarker [a,1], Sonia Kiran [a], Yan Li [b,c], Qing-Xiang Amy Sang [a,c,*]

[a] Department of Chemistry and Biochemistry, Florida State University, Tallahassee, FL, 32306-4390, USA
[b] Department of Chemical and Biomedical Engineering, FAMU-FSU College of Engineering, Florida State University, Tallahassee, FL, 32310-6046, USA
[c] Institute of Molecular Biophysics, Florida State University, Tallahassee, FL, 32306-4380, USA

ARTICLE INFO

Keywords:
Atypical teratoid/rhabdoid tumor
Human induced pluripotent stem cells
CRISPR/Cas9 gene editing
Tumor suppressor genes
SMARCB1
Brain tumor modeling

ABSTRACT

Atypical teratoid/rhabdoid tumor (ATRT) is a rare childhood malignancy that originates in the central nervous system. Over ninety-five percent of ATRT patients have biallelic inactivation of the tumor suppressor gene *SMARCB1*. ATRT has no standard treatment, and a major limiting factor in therapeutic development is the lack of reliable ATRT models. We employed CRISPR/Cas9 gene-editing technology to knock out *SMARCB1* and *TP53* genes in human episomal induced pluripotent stem cells (Epi-iPSCs), followed by brief neural induction, to generate an ATRT-like model. The dual knockout Epi-iPSCs retained their stemness with the capacity to differentiate into three germ layers. High expression of *OCT4* and *NANOG* in neurally induced knockout spheroids was comparable to that in two ATRT cell lines. Beta-catenin protein expression was higher in SMARCB1-deficient cells and spheroids than in normal Epi-iPSC-derived spheroids. Nucleophosmin, Osteopontin, and Ki-67 proteins were also expressed by the SMARCB1-deficient spheroids. In summary, the tumor model resembled embryonal features of ATRT and expressed ATRT biomarkers at mRNA and protein levels. Ribociclib, PTC-209, and the combination of clofilium tosylate and pazopanib decreased the viability of the ATRT-like cells. This disease modeling scheme may enable the establishment of individualized tumor models with patient-specific mutations and facilitate high-throughput drug testing.

1. Introduction

An atypical teratoid/rhabdoid tumor (ATRT) originates as a malignant rhabdoid tumor of the central nervous system. Its cellular origin is largely unknown, perhaps early neural progenitor cells (NPCs) [1,2]. ATRT predominantly affects children and infants with biallelic inactivation of a tumor suppressor gene SWI/SNF-related, matrix-associated, actin-dependent regulator of chromatin, subfamily B, member 1 (*SMARCB1*) [3–5]. Children younger than three years of age constitute 80% of aggressive ATRT cases, with a low 5-year survival rate of 32.2% [6]. There exists no consensus on a standard treatment for ATRT; however, chemotherapy and surgical resections are the most commonly employed therapies [7–10]. Still, the recurrence rate in ATRT patients is high, and recurrent tumors show more aggressive self-renewal and invasive properties through an activated signal transducer and activator of the transcription 3 (STAT3)/Snail pathway [11,12]. Radiation is effective for more aggressive cancers in children under three years old, but it causes neurotoxicity and involves high-risk protocols [10]. Hence, safe and effective treatment for ATRT is an unmet medical need. One major factor that limits the understanding of molecular mechanisms of ATRT and concordant therapeutic development is the lack of reliable ATRT models for drug target identification and therapeutic evaluation.

Since SMARCB1 is a core component of the SWI/SNF chromatin-remodeling complex, its inactivation results in deranged

Peer review under responsibility of KeAi Communications Co., Ltd.
* Corresponding author. Institute of Molecular Biophysics, Florida State University, Tallahassee, FL, 32306-4380, USA.
E-mail addresses: tph16c@fsu.edu (T. Hua), yx21@fsu.edu (Y. Xue), ds22@fsu.edu (D.B. Sarker), skiran@fsu.edu (S. Kiran), yli4@fsu.edu (Y. Li), qxsang@chem.fsu.edu (Q.-X.A. Sang).
[1] These authors contributed equally to this work.
[2] Current address: Department of Hematology and Medical Oncology, Winship Cancer Institute of Emory University, Emory University School of Medicine, Atlanta, GA 30322.

https://doi.org/10.1016/j.bioactmat.2023.08.009
Received 24 April 2023; Received in revised form 2 August 2023; Accepted 8 August 2023

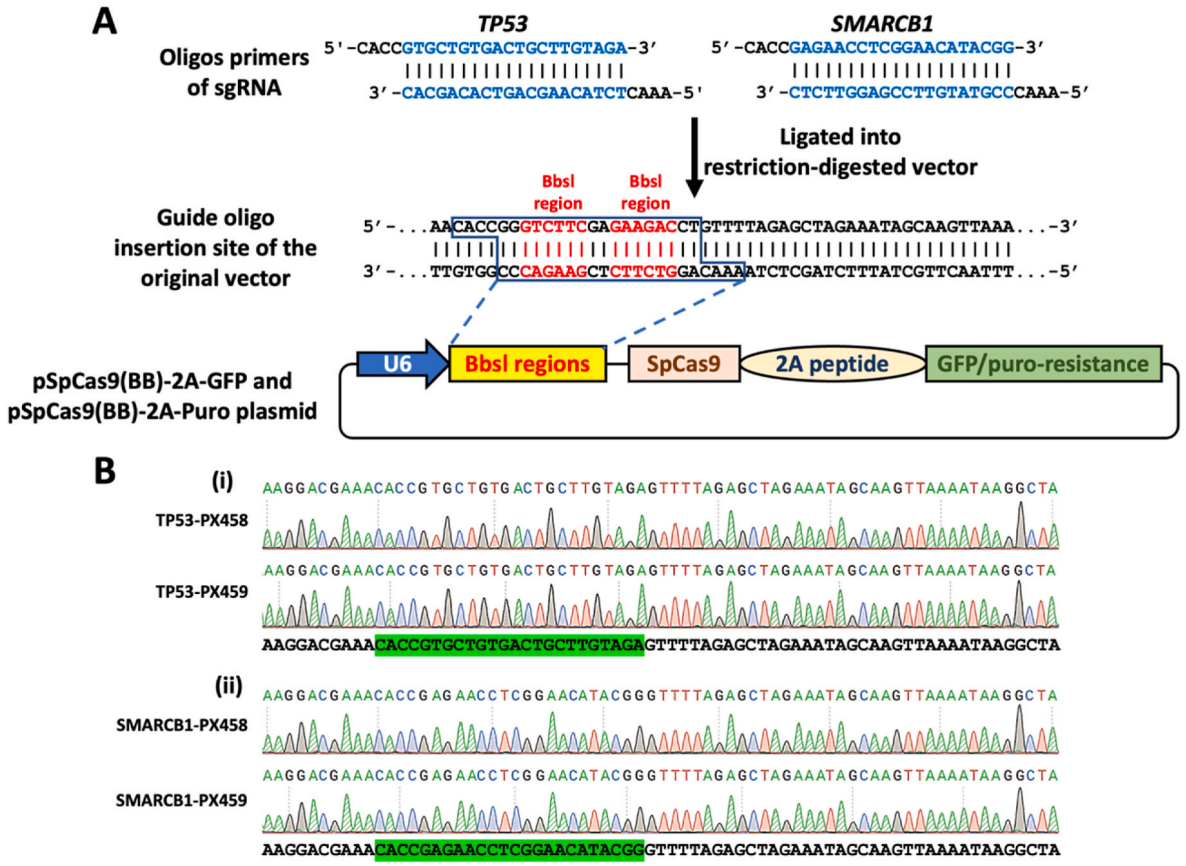

Fig. 1. Insertion of guide RNA oligos into PX458 and PX459 vectors. (A) Oligos for single guide RNA (sgRNA) targeting *TP53* and *SMARCB1* genes were inserted separately into the BbsI regions of two different vectors, PX458 (GFP) and PX459 (Puromycin resistance), to construct a total of 4 distinct plasmids. **(B)** These plasmids were checked for the presence of the sgRNA-coding sequences that targets **(i)** *TP53* and **(ii)** *SMARCB1*. The green highlighted sequences are the inserts for sgRNA.

transcriptional regulation and concomitant rhabdoid tumor formation [13]. SMARCB1 is a tumor suppressor protein that regulates the canonical Wnt and sonic hedgehog (SHH) pathway and activates p16-INK4a and retinoblastoma tumor suppressor protein (RB1) [4]. SMARCB1 inactivation reduces the binding potential of the transcription factor T-cell factors (TCF) to the Wnt/β-catenin promoter and causes its target genes to be overexpressed [14]. Also, SMARCB1 directly interacts with glioma-associated oncogene homolog 1 (GLI1) by controlling chromatin structure at the GLI1 target promoter and lowering the expression of its target genes, including *Ptch1* and *Gli1* itself in mice [15]. ATRT exhibits an elevated expression of the SHH-GLI1 pathway genes, and GLI1 is needed for rhabdoid tumor cell proliferation and colonization [15]. In addition, SMARCB1 inhibits cell cycle progression to the S phase, which can be countered by sequential phosphorylation of RB1 through cyclin D1–cyclin-dependent kinase (CDK) 4 or 6 and cyclin E-CDK2 complexes [16]. The hyperphosphorylated RB1 disrupts the RB1-E2F stability and releases the E2F transcription factor to activate its target genes that permit cells to enter the S phase and undergo mitosis [17,18]. Moreover, RB1 and p16-INK4a inhibit tumor growth by suppressing gene expression and inhibiting cyclin D1-CDK4/6 independent of SMARCB1 [16,19].

Human pluripotent stem cells (hPSCs) include human embryonic stem cells (hESCs) and human induced pluripotent stem cells (hiPSCs). The hPSCs can differentiate into three germ layers, forming organoids similar to human tissue and organs [20–22]. Brain organoids resembling distinct brain regions have been successfully developed *in vitro* using chemical and physical inductions to form a 3D culture, which allows for cell-cell and cell-matrix interaction and physiological activities [23–25]. These organoids present an excellent platform for neurological disease modeling and drug screening [26]. Genetically engineered cerebral organoids derived from hiPSCs could recapitulate every glioblastoma subtype [27]; however, hiPSC-derived ATRT tumor models are yet elusive. Fibroblast growth factor 2 (FGF2) can induce neuronal differentiation of hiPSCs, but extended induction may promote the acquisition of epithelial phenotype by the neural progenitor cells [28]. ATRT likely originates from early NPCs whose marker is Nestin; therefore, the timing for SMARCB1 inactivation is crucial for generating cancerous brain organoids [1,29]. Hence, on the hypothetical premise that ATRT originates from early NPCs, we inactivated SMARCB1 in hiPSCs to build a novel early-stage brain tumor model like ATRT to study its molecular characteristics and evaluate therapeutics.

We utilized clustered regularly interspaced short palindromic repeats (CRISPR)-associated protein 9 (Cas9) to target *TP53* and *SMARCB1* genes in human episomal iPSCs (Epi-iPSCs) to build an ATRT-like model. CRISPR/Cas9 genome editing tool was used to mutate the target genes in footprint- and transgene-free Epi-iPSCs. When *SMARCB1* was mutated first in the Epi-iPSCs, the cells did not survive. So, we considered mutating *TP53*, another tumor suppressor gene that plays a critical role in cell growth and prevents cancer cell formation [30]. We hypothesized that inactivating the function of both TP53 and SMARCB1 preceding neural induction could be crucial for generating the ATRT-like model. So, we mutated *TP53* before knocking out *SMARCB1* and let edited Epi-iPSCs undergo short neural induction to produce ATRT-like spheroids for biomarker study and drug testing.

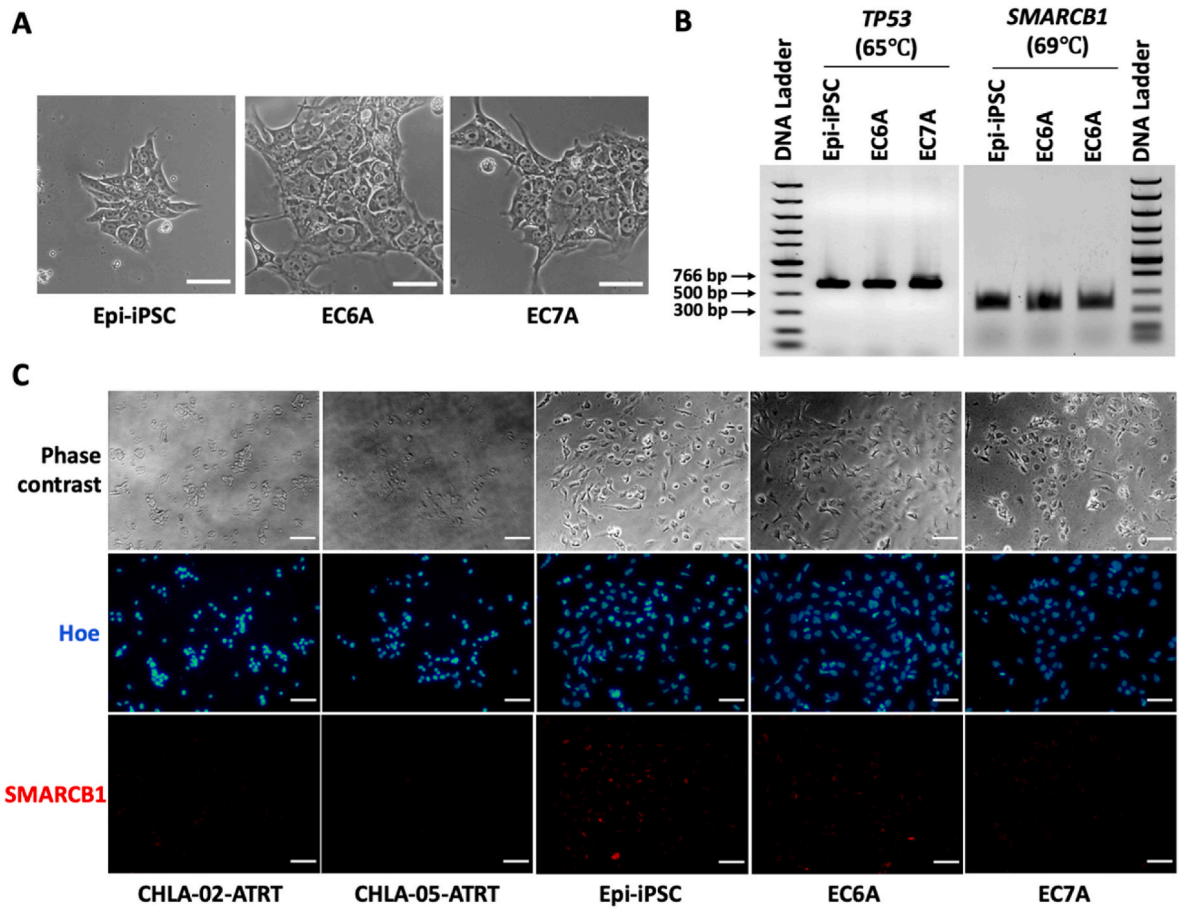

Fig. 2. Assessment of morphology, on-target plasmid DNA insertion, and nuclear SMARBC1 expression in knockout clones. (A) Phase contrast images of normal Epi-iPSC, EC6A, and EC7A show no major morphological differences. **Scale bar: 25 μm**. **(B)** Target DNA amplification yielded PCR products of 604 bp (*TP53*) and 341 bp (*SMARCB1*), implying no on-target plasmid DNA insertion. **(C)** SMARCB1 staining in two negative control cell lines, CHLA-02-ATRT and CHLA-05-ATRT; one positive control, Epi-iPSC; and two SMARCB1 knockout clones, EC6A and EC7A. **Scale bar: 50 μm.**

2. Materials and methods

2.1. Human induced pluripotent stem cell and ATRT cell culture

Human episomal iPSC (Epi-iPSC, ThermoFisher, Cat#: A18945) expresses seven factors (SOKMNLT; SOX2, OCT4, KLF4, MYC, NANOG, LIN28, and SV40L T antigen), has no footprints, and is free of all reprogramming genes. The cells were cultured using mTeSR™ Plus Basal Medium (STEMCELL Technologies, Cat#: 100–0274) and passaged when they reached 80% confluency using Accutase® (Innovative Cell Technologies, Cat#: 10210-214). The cells were split into a 1:8–1:10 ratio for new culture per well of a 6-well plate with the rho-associated, coiled-coil containing protein kinase inhibitor (ROCKi) Y-27632 (10 μM, Sigma) for 24h.

The patient-derived ATRT cell lines used were CHLA-02-ATRT (ATCC, Cat#: CRL-3020) from a 20-month-old male and CHLA-05-ATRT (ATCC, Cat#: CRL-3037) from a 2-year-old male. Both cell lines were cultured in ultra-low attachment plates. The base medium for both the cell lines was Dulbecco's Modified Eagle Medium (DMEM)/Nutrient Mixture F-12 (DMEM/F12) (ATCC, Cat#: 30–2006) with 1x B-27 Supplement (Gibco, Cat#: 17504044), 20 ng/mL epidermal growth factor (EGF) (Gibco, Cat#: PHG0311), and 20 ng/mL fibroblast growth factor 2 (FGF2) (Gibco, Cat#: PHG0021). Accumax® (Innovative Cell Technologies, Cat#: AM-105) was used to dissociate aggregates of these ATRT cell lines.

2.2. Designing CRISPR/Cas9 plasmids that target SMARCB1 and TP53 genes

The vectors pSpCas9(BB)-2A-GFP (PX458) and pSpCas9(BB)-2A-Puro (PX459) were ordered from Addgene. The vectors were digested with the BbsI enzyme overnight at 37 °C for preparation. Gel extraction was used to obtain the linear product of vector digestion. Negative control of ligation was set up to check for background. Also, 10 μM oligo primer pairs (*TP53*: 5′-CACC GTGC TGTG ACTG CTTG TAGA-3′ and 3′-CACG ACAC TGAC GAAC ATCT CAAA-5'; *SMARCB1*: 5′-CACC GAGA ACCT CGGA ACAT ACGG-3′ and 3′-CTCT TGGA GCCT TGTA TGCC CAAA-5'; designed using https://zlab.bio/guide-design-resources) were combined in a 0.2 mL PCR tube or strip for oligos preparation. The annealing cycle was done as follows: 95 °C for 5 min, 85 °C for 1 min, 75 °C for 1 min, 65 °C for 1 min, 55 °C for 1 min, 45 °C for 1 min, 35 °C for 1 min, 25 °C for 1 min, and on hold at 4 °C. The annealed oligos were then diluted in H_2O at a ratio of 1:22 and ligated in a 10 μL reaction of 50 ng digested vector, 1.0 μL of diluted annealed oligo mix for 30 min at room temperature, and then 2 min on ice. The 5 μL ligation reaction was transformed in DH5α cells before plating 100 μL cell suspension on an appropriate antibiotic plate and incubating overnight at 37 °C. The plasmid sequence was read using U6 promoter primers, and the results were analyzed using BioEdit (http://www.mbio.ncsu.edu).

2.3. Transfection of the Epi-iPSCs

Lipofectamine™ 3000 (ThermoFisher, Cat#: L3000001) was used to

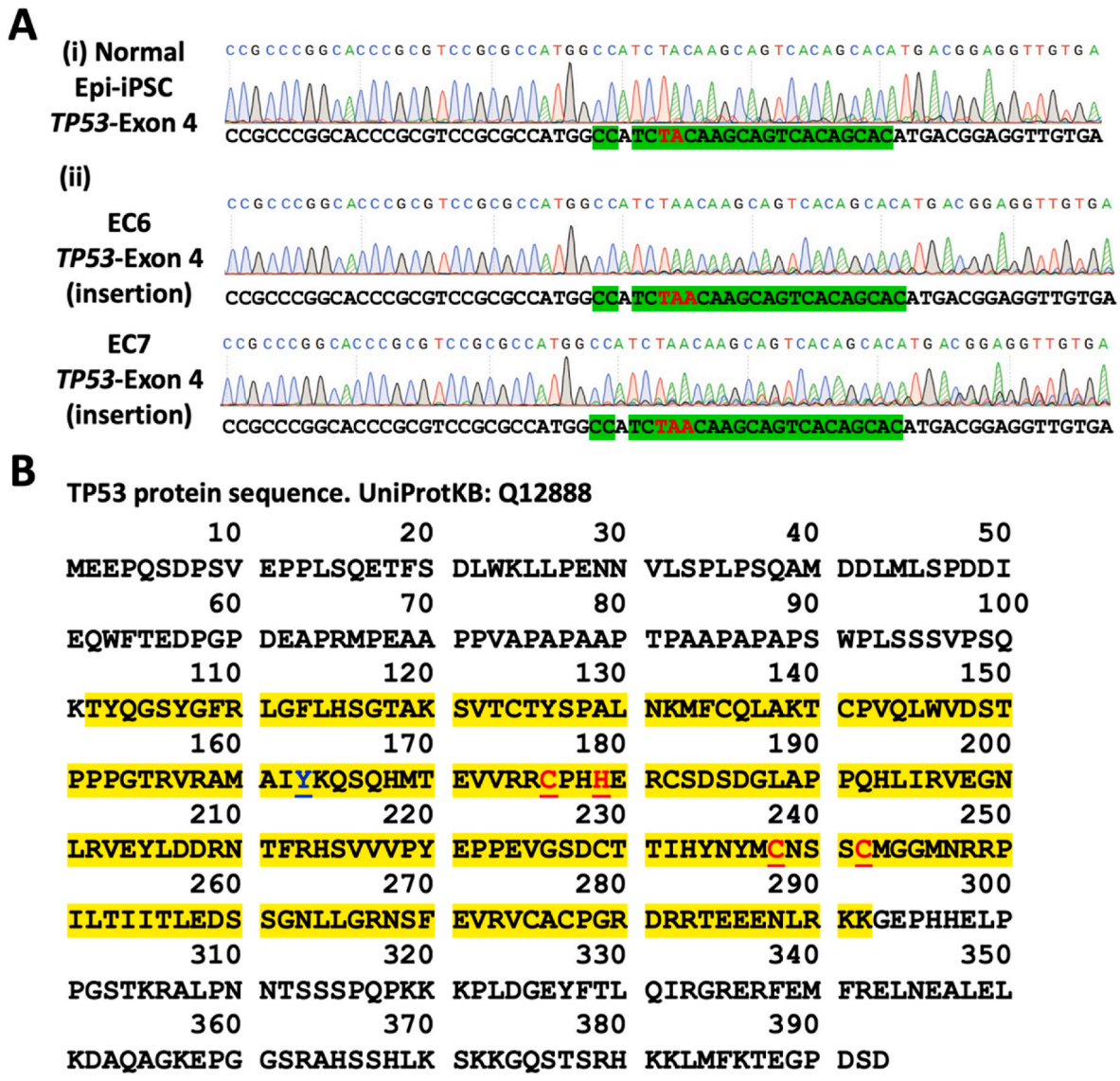

Fig. 3. Sequencing around the *TP53* target site for the clones (A) *TP53* target site was sequenced for **(i)** normal Epi-iPSC and **(ii)** *TP53*-knockout EC6 and EC7 clones to confirm the addition of an extra adenosine nucleotide to exon 4 in knockout cells. **(B)** TP53 protein contains a DNA binding region (highlighted in yellow) and Zn^{2+} binding amino acids (underlined red). EC6 and EC7 clones with the additional adenosine nucleotide in the *TP53* gene have a premature stop codon in place of Tyr163 (underlined blue).

transfect Epi-iPSCs to generate *TP53* and *SMARCB1* mutations following the manufacturer's protocol. Briefly, Opti-MEM™ (ThermoFisher, Cat#: 31985062) was used to dilute the Lipofectamine™ 3000 solution and DNA-P3000™ complex at room temperature. The two mixtures were then combined and left alone for 5 min to form a lipid-DNA complex before being added to the culture at 30% confluence. The selection of PX459-transfected cells was done using 1 μg/mL puromycin after 24 h of transfection. The transfected Epi-iPSCs were diluted into varying concentrations in a 96-well plate. The wells with single-cell colonies were used for further characterization.

Cells transfected with the GFP marker containing plasmid (PX458) were collected and sorted using the 488 nm laser of the FACS SORP instrument at Florida State University. The data were analyzed using FlowJo. In addition, some of the cells were plated on a 96-well plate before PX458 transfection. After 24 h and 48 h, fluorescence images were taken using a fluorescent microscope (Olympus IX70, Melville, NY).

2.4. Spheroid differentiation from Epi-iPSCs

Dual knockout Epi-iPSCs were subjected to neural induction to obtain an ATRT-like model. Before the induction, cells were maintained in mTeSR Plus Basal Medium (STEMCELL, Cat#: 100–0274) with antibiotics and 1x mTeSR Plus Supplement (STEMCELL, Cat#: 100–0275). On day 0, cells were dissociated by Accutase®, and 5×10^4 cells were seeded per well of a low attachment 24-well plate (Corning, Cat#: 3473) in DMEM/F-12 (ThermoFisher, Cat#: 11320033) containing 2% B-27 supplement (ThermoFisher, Cat#: 17504044), 100 U/mL penicillin, 100 μg/mL streptomycin, 10 μM transforming growth factor (TGF)-beta inhibitor, SB431542, and 10 μM ROCKi, Y-27632. After 48 h, the media was changed, and 50 ng/mL FGF2 was added to promote neural induction for spheroid formation until day 7 for characterization.

For RT-PCR, day-7 spheroids were collected and centrifuged at 300×*g* for 5 min. Then, the total mRNA was isolated from the spheroids using RNeasy® Mini Kit (Qiagen, Valencia, CA), concentrated, and cleaned using the RNA Clean & Concentrator-5 kit (Zymo, Irvine, CA).

For immunocytochemistry, the spheroids were collected and treated

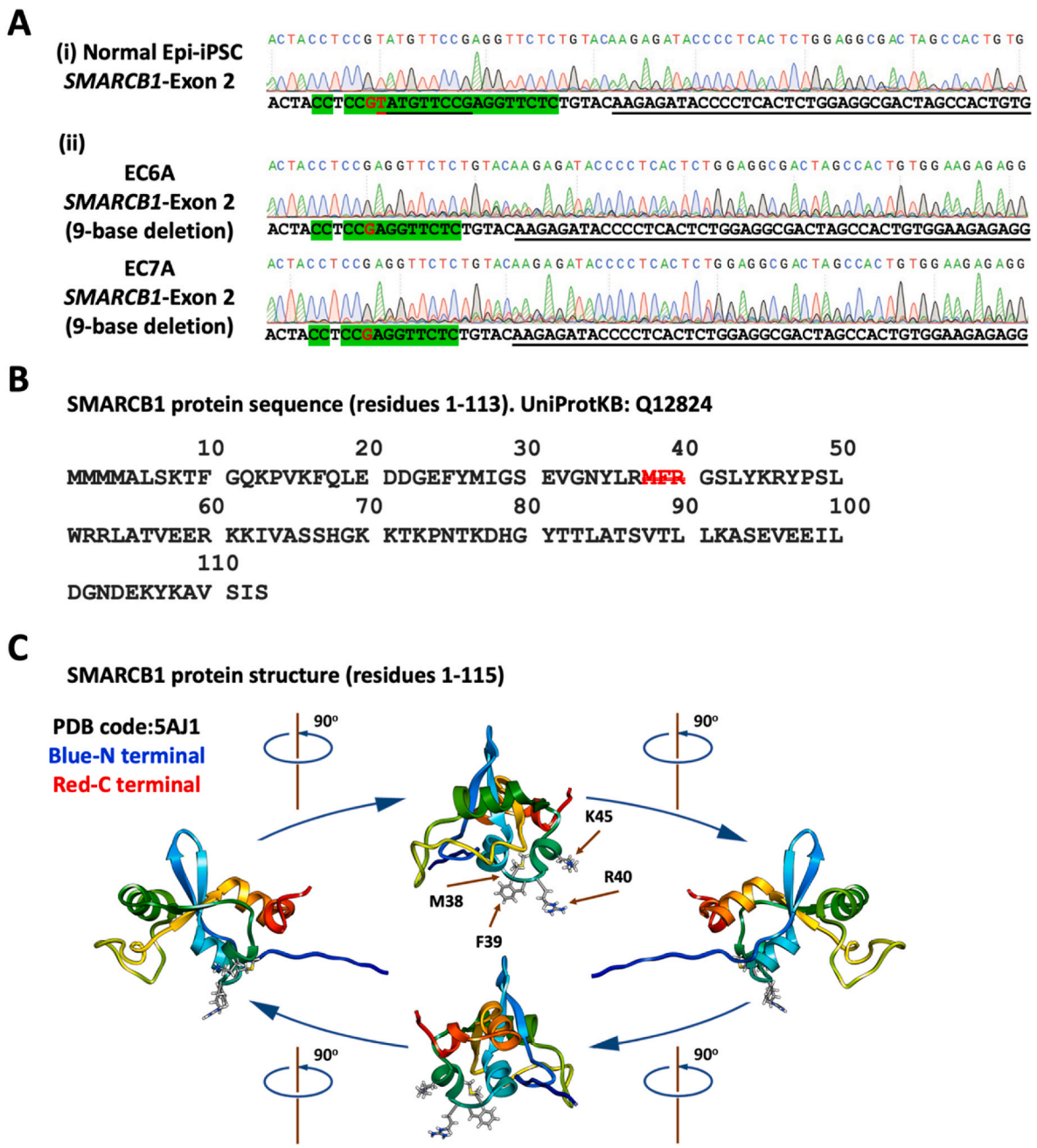

Fig. 4. Sequencing around the *SMARCB1* target site for the clones. **(A)** *SMARCB1* target site was sequenced for **(i)** normal Epi-iPSC and **(ii)** dual-knockout EC6A and EC7A clones to confirm the deletion of 9 nucleotides from exon 2 in knockout clones. **(B)** The deleted nucleotides affected three contiguous codons for the amino acids Met38-Phe39-Arg40 (strikethrough and red-colored). **(C)** The cartoon representation of the first 115 amino acids of SMARCB1. They are highly conserved across metazoans and possibly bind DNA.

with Accumax® at 37 °C for 15 min. The dissociated cells were replated on a Matrigel-coated surface for 48 h before being fixed and probed for markers of interest.

2.5. Immunocytochemistry (ICC)

Cells and spheroids were plated on *Matrigel*™-coated 96-well plates before being fixed with 4% paraformaldehyde (PFA). Then, 0.1% triton X-100 solution in phosphate-buffered saline (PBS) was used to permeabilize the cell membrane for intracellular markers. Next, the samples were blocked in 2% fetal bovine serum (FBS) in PBS before being treated with primary and matched secondary antibodies (Supplementary Table S1). The samples were counterstained with Hoechst 33342 and visualized using a fluorescent microscope (Olympus IX70, Melville, NY).

2.6. Polymerase chain reaction and DNA sequencing

Genomic DNA content was extracted for analysis using the E.Z.N.A.® Tissue DNA kit (Omega Bio-Tek). The DNA concentration was determined using a NanoDrop™ instrument. Polymerase chain reaction (PCR) was performed using different primers that target the exons of interest (Supplementary Table S2). Genomic changes were checked using One*Taq*® Quick-Load® 2X Master Mix with Standard Buffer (New England BioLabs). The amplification cycle was done as follows: 94 °C (1 min); 35 cycles of 94 °C (1 min), 60 °C (30 s), and 68 °C (3 min); 68 °C (1 min); and on hold at 4 °C. 1% Agarose gel with ethidium bromide was

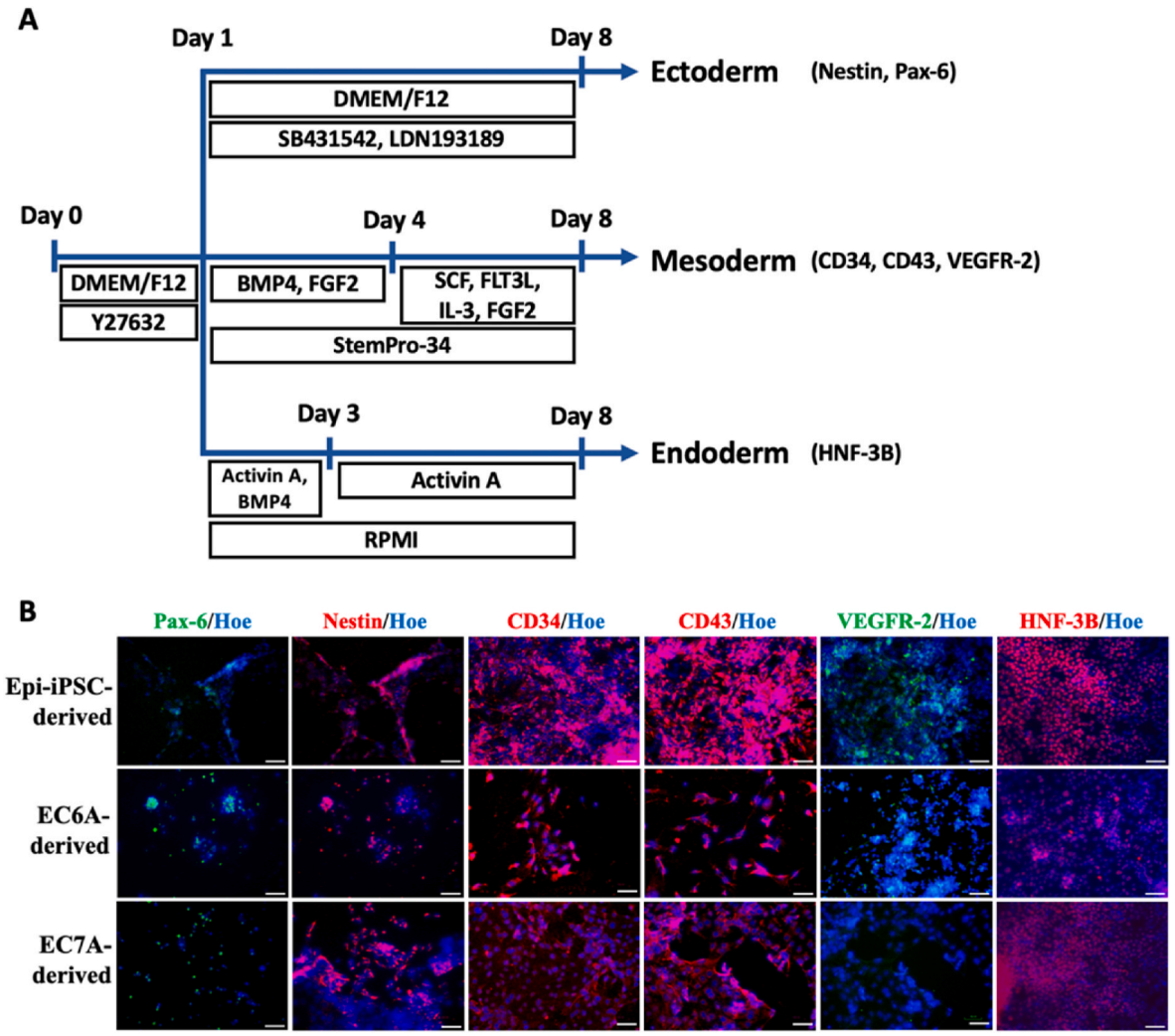

Fig. 5. Differentiation capacity of EC6A and EC7A. (A) Schematic illustration of germ layer differentiation protocols. 10 μM of ROCK inhibitor was added to the human iPSCs, EC6A, and EC7A in the first 24 h. The endoderm differentiation was performed in RPMI medium with Activin A and BMP4. On day 3, the media was changed to fresh media with only Activin A till day 8. For the mesoderm differentiation, the cells were cultured in StemPro™-34 with factors BMP4 and FGF2 on day 1. These factors were replaced on day 4 with SCF, FLT3L, IL-3, and FGF2 till day 8. For the ectoderm differentiation, the cells were plated in DMEM/F12 with SB431542 and LDN193189 from day 1 to day 8. **(B)** Immunostaining reveals the expression of germ layer-specific markers by both clones. CD34, CD43, and VEGFR-2 are markers for mesoderm. HNF–3B is an endoderm marker. The markers for ectoderm are Pax-6 and Nestin. Separate ICC images for each marker can be found in Supplementary Fig. S5. BMP4: bone morphogenetic protein 4; FGF2: fibroblast growth factor 2; SCF: stem cell factor; FLT3L: FMS-like tyrosine kinase 3 ligand; IL-3: interleukin 3; CD34: hematopoietic progenitor cell antigen CD34; CD43: leukosialin; VEGFR-2: vascular endothelial growth factor receptor 2; Pax-6: paired box protein Pax-6; HNF–3B: hepatocyte nuclear factor 3-beta; Hoe: Hoechst 33342. **Scale bar: 50 μm**.

used for the electrophoresis of the PCR products. DNA was sequenced using Sanger sequencing on an ABI-3730 at Florida State University using primers that would detect the shorter sequences within the PCR products (Supplementary Table S2).

Q5® High-Fidelity 2X Master Mix (New England BioLabs) can amplify approximately 30-kilobase (kb) DNA sequence in 5 min, so it was used to determine if there was any large insertion or deletion after transfection. Forward primers for *TP53* and *SMARCB1* exon amplification were used for this purpose (Supplementary Table S2). The PCR condition for *TP53* was 94 °C (1 min); 35 cycles of 94 °C (1 min), 65 °C (30 s), and 72 °C (5 min); 72 °C (10 min); and on hold at 4 °C. For *SMARCB1*, it was 94 °C (1 min); 35 cycles of 94 °C (1 min), 69 °C (30 s), and 72 °C (5 min); 72 °C (10 min); and on hold at 4 °C.

2.7. SMARCB1 structure visualization

The structure of SMARCB1's first 115 amino acids was obtained from the PDB database (https://www.rcsb.org/structure/5AJ1) [31]. Structure visualization was done using the software Chimera 1.16 (https://www.cgl.ucsf.edu/chimera/).

2.8. Three germ layer differentiation

For three germ layer differentiation, 10 μM of ROCKi was added to the normal Epi-iPSCs and dual knockout Epi-iPSC clones (EC6A and EC7A) in the first 24 h. Endoderm differentiation was performed in Roswell Park Memorial Institute (RPMI) 1640 medium containing 2% B27 with 50 ng/mL Activin A and 50 ng/mL bone morphogenetic protein 4 (BMP4). On day 3, the media was replaced with the fresh RPMI media supplemented with 2% B27 and 50 ng/mL of Activin A till day 8. For mesoderm differentiation, the cells were plated in StemPro™-34 serum-free media (Invitrogen) with 2 mM L-glutamine, 1% nonessential amino acids, 10 μM of 2-mercaptoethanol, 100 U/mL penicillin, 100 μg/mL streptomycin, and 50 mg/mL ascorbic acid. The cells were cultured in 30 ng/mL human BMP4 and 5 ng/mL human FGF2 on day 1. These growth factors were replaced on day 4 with 100 ng/mL stem cell factor

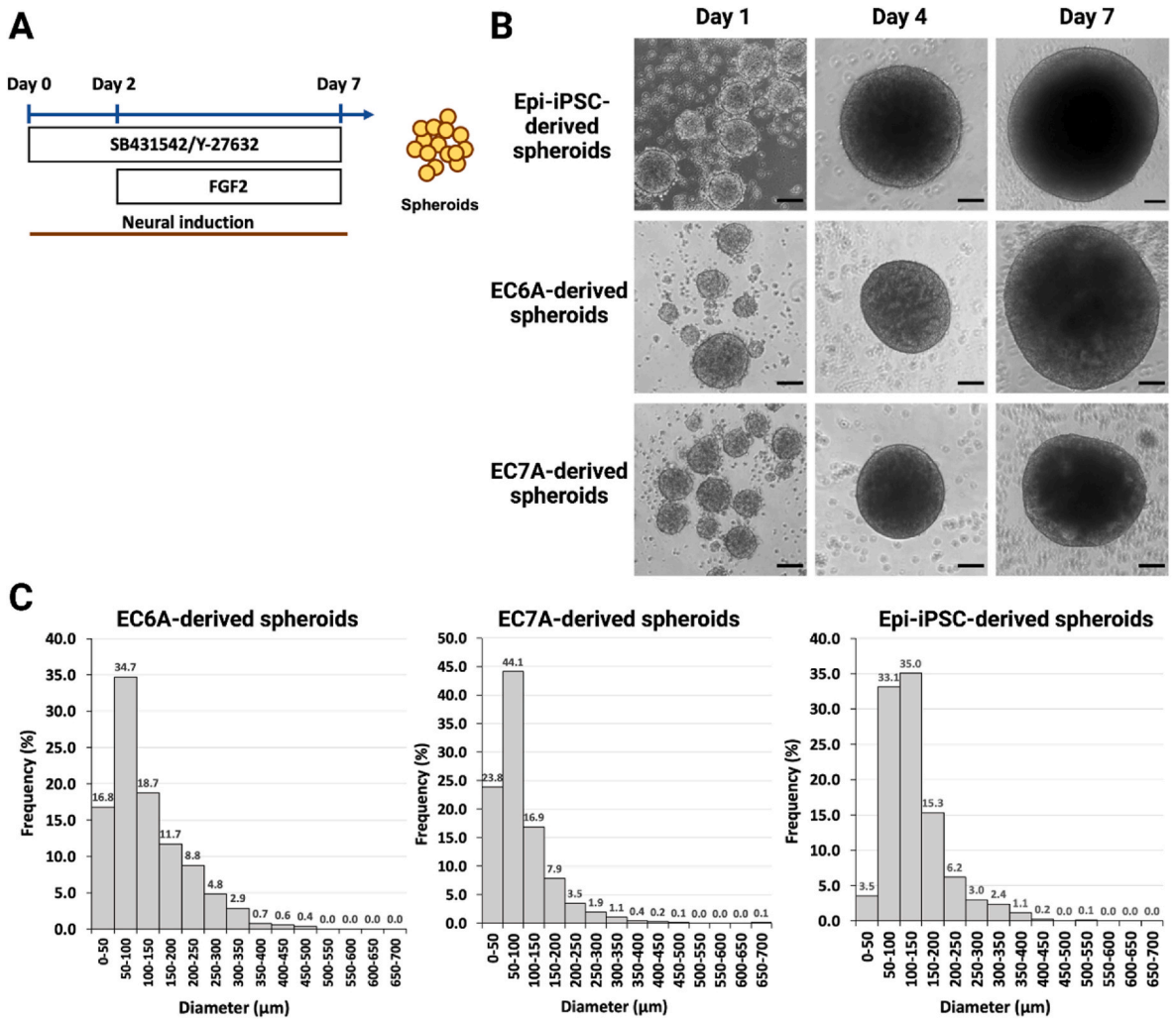

Fig. 6. Neural induction of Epi-iPSC, EC6A, and EC7A. (A) Schematic illustration of the neural induction procedure. SB431542 is the inhibitor of the transforming growth factor (TGF)-beta, and Y-27632 is the inhibitor of rho-associated protein kinase signaling pathway. **(B)** Phase contrast images of spheroids undergoing neural induction at days 1, 4, and 7. **(C)** The size distribution of EC6A-derived spheroids (n = 1084), EC7A-derived spheroids (n = 1233), and Epi-iPSC-derived spheroids (n = 876). **Scale bar: 50 μm**.

(SCF), 20 ng/mL human FMS-like tyrosine kinase 3 ligand (FLT3L), 20 ng/mL human interleukin 3 (IL-3), and 5 ng/mL FGF2 till day 8. Similarly, for ectoderm differentiation, the cells were plated in DMEM/F12 containing 2% B27, 10 μM SB431542, and 100 nM LDN193189 from day 1 to day 8. Cells were always on *Matrigel*™ for endoderm differentiation due to the low viability in suspension. Ectoderm and mesoderm differentiation was carried out on low-attachment plates. Upon completion of differentiation, the cells were replated on a 96-well plate, and select markers specific to each germ layer were investigated using immunocytochemistry. The markers were hematopoietic progenitor cell antigen CD34, leukosialin (CD43), and vascular endothelial growth factor receptor 2 (VEGFR-2) for mesoderm; paired box protein Pax-6 and Nestin for ectoderm, and hepatocyte nuclear factor 3-beta (HNF–3B) for endoderm. A list of molecules used for differentiation can be found in Supplementary Table S3.

2.9. Calcium signaling assay

Human iPSC-, EC6A-, and EC7A-derived spheroids were dissociated with Accumax® (STEMCELL Technologies) and plated on a 96-well plate overnight in triplicates. The cell media was removed, and the cells were washed with the assay buffer. The assay buffer contained 100 μL of 1x Fluo-4 dye (Life Technologies). 2.5 mM probenecid was added to each well, and the cells were incubated at 37 °C for 30 min. The cells were then kept at room temperature for an additional 30 min. Background signal was measured in the first 60 s, and then 20 μM of adenosine 5′-diphosphate (ADP, Sigma) solution was added to the assay buffer (without probenecid). The calcium transients were captured every 30 s for another 210 s using a fluorescent microscope (Olympus IX70, Melville, NY).

2.10. Reverse transcription-polymerase chain reaction (RT-PCR)

Spheroids were collected, and the total mRNA samples were isolated using RNeasy® Mini Kit (Qiagen, Valencia, CA). It was followed by RNA concentration and clean-up steps using RNA Clean & Concentrator-5 kit (Zymo, Irvine, CA). About 1 μg of total RNA was used for reverse transcription. cDNA was synthesized using the Superscript™ III kit (Invitrogen, Carlsbad, CA) with oligo-dT primers. The qPCR primers for the markers of interest (Supplementary Table S4) were designed using Primer-BLAST (https://www.ncbi.nlm.nih.gov/tools/primer-blast/), and their melting points were checked using NetPrimer (https://www.premierbiosoft.com/netprimer/). The β-actin gene was used as an endogenous control and for the normalization of expression levels of all the other markers. The RT-PCR experiment was done using an ABI7500 instrument (Applied Biosystems, Foster City, CA) or AB Quantstudio 7

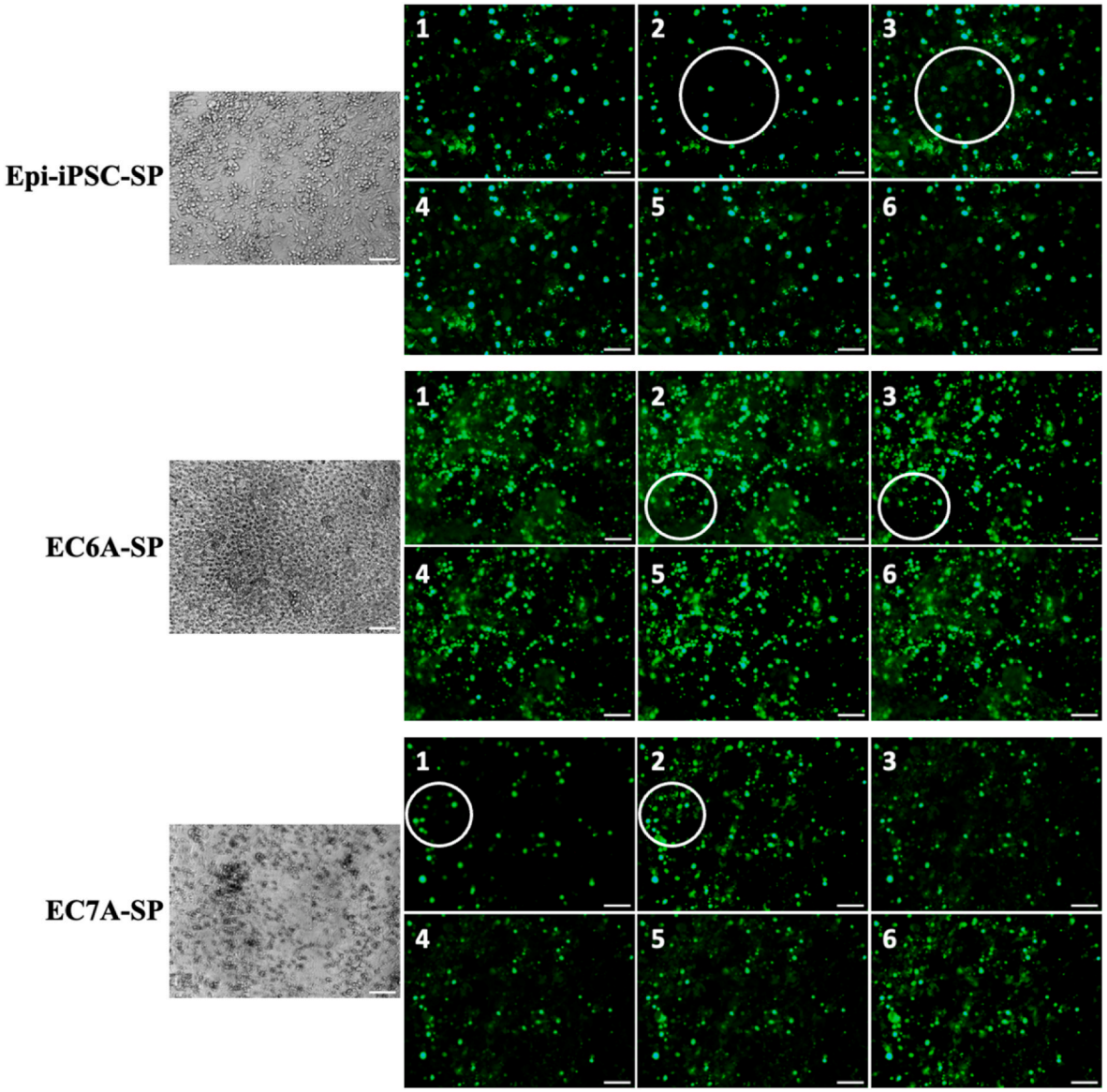

Fig. 7. Live-cell images of Epi-iPSC-, EC6A-, and EC7A-derived spheroid cells with intracellular calcium transients. On day 7, spheroids were dissociated and cultured on *Matrigel*™ for 24 h. The transients were measured every 30 s using a fluorescent microscope with 20x magnification. Noticeable signal changes between two frames are circled. **Scale bar: 50 μm.**

flex, both machines using SYBR Green PCR Master Mix (Applied Biosystems). The amplification was performed in a sequence at 50 °C (2 min); 95 °C (10 min); 40 cycles of 95 °C (15 s), 55 °C (30 s), and 68 °C (30 s). The C_t values of the target genes were normalized to the C_t values of the endogenous control β-actin. The corrected C_t values were then compared for the knockout and control spheroids. Fold changes in gene expression were calculated using the comparative C_t method: $2^{-(\Delta Ct\ sample - \Delta Ct\ control)}$ to obtain the relative expression levels.

2.11. MTT (3-(4,5-dimethylthiazol-2-yl)-2,5-diphenyltetrazolium bromide) assay

Human iPSC-, EC6A-, and EC7A-derived spheroids were dissociated and replated at 3×10^4 cells/well of a 96-well plate to test the drug effects after 48 h of treatment. MTT in PBS was added to the cells, and the culture was incubated for 40 min. The cells were collected, washed with PBS, and treated with sodium dodecyl sulfate (SDS) to dissolve formazan. The absorbance of the formazan solution was measured at 570 nm. The data were analyzed using SigmaPlot to determine the half-maximal inhibitory concentration (IC_{50}) values. The assay was performed for drug-treated CHLA-02-ATRT and CHLA-05-ATRT cell lines for drug response comparison with the ATRT-like model.

2.12. Flow cytometry

Cells were dissociated by Accutase®. About 1×10^6 cells were used to characterize each marker. The cells were fixed with 10% formalin buffer (ThermoFisher), permeabilized for intracellular markers, and then incubated with primary antibodies followed by secondary antibodies. The samples were analyzed using BD FACSCanto™ II flow cytometer (Florida State University College of Medicine). The data were analyzed using the FlowJo software.

2.13. Drug treatment

Day-7 spheroids were dissociated, and the cells were replated on a Matrigel-coated surface in a 96 well-plate overnight. The next day, ribociclib, PTC209, and the combination of clofilium tosylate and

Table 1
ATRT biomarkers for model characterization via RT-PCR. *GLI1*: glioma-associated oncogene family zinc finger 1; *GLI2*: glioma-associated oncogene family zinc finger 2; *GSK3B*: glycogen synthase kinase 3 beta; *CTNNB1*: catenin beta-1; *LEF1*: lymphoid enhancer binding factor 1; *OCT4*: octamer-binding protein 4; *NANOG*: Nanog homeobox; *ENO2*: enolase 2; *NEPH3*: kirre-like nephrin family adhesion molecule; *IDH1*: isocitrate dehydrogenase NADP(+) 1; *OPN*: osteopontin; *RB1*: retinoblastoma transcriptional corepressor 1; *MKI67*: marker of proliferation Ki-67; *STAT3*: signal transducer and activator of transcription 3.

Marker type	Gene	Description of the encoded protein
SHH pathway	***GLI1***	A transcription factor of the SHH pathway
	GLI2	A transcription repressor of the SHH pathway
β-catenin pathway	***GSK3B***	Forms complex with other proteins to phosphorylate CTNNB1 for proteosome-mediated degradation
	CTNNB1	Acts as a cell-cell adhesion protein and participates in canonical Wnt signaling pathway for gene transcription
	LEF1	A transcription factor of the canonical Wnt signaling pathway
Embryonic	***OCT4***	Makers of pluripotent stem cells
	NANOG	
Neuronal	***ENO2***	Neuron-specific enolase
	NEPH3	A marker of the molecular layer of the cerebellum
Potential ATRT biomarkers	***IDH1***	Catalyzes the oxidative decarboxylation of isocitrate to 2-oxoglutarate
	OPN	An extracellular structural protein that is highly expressed in rhabdoid tumors
	RB1	A tumor suppressor marker and negative regulator of the cell cycle
	MKI67	Marker of cell proliferation
	STAT3	Expressed in drug-resistant ATRT cells

pazopanib were treated at concentrations of 100, 50, 10, 5, 6.25, 1, 0.5, 0.1, 0.05, and 0.01 μM. DMSO was used as the control treatment. After two days, MTT assay was performed to measure cell viability.

2.14. Statistical analysis

RT-PCR, cell proliferation, and cell viability results were represented as [mean ± standard deviation]. In addition, they were repeated as three independent data points (n = 3). To compare two conditions, Student's t-test was used to determine the significance. A p-value <0.05 was considered significant. On the other hand, for comparing more than two different conditions, a one-way analysis of variance (ANOVA) was used, followed by Tukey's post hoc test. A cutoff p value of 0.05 was used to determine statistical significance.

3. Results

3.1. Dual knockout Epi-iPSCs retained differentiation capacity and formed spheroids upon neural induction

The oligo pairs of interest were annealed before transferring into the BbsI regions of the plasmid (Fig. 1A). The guide RNA with the scaffold was expressed during the mRNA synthesis steps. The Cas9 protein and markers for selection, either green fluorescent protein or puromycin-N-acetyltransferase, were synthesized during the protein synthesis. Puromycin-N-acetyltransferase would confer puromycin resistance to the transfected cells. The plasmids were sequenced to verify that the oligonucleotides were successfully ligated into the vectors for knocking out *TP53* (Fig. 1B(i)) and *SMARCB1* (Fig. 1B(ii)). The plasmid with green fluorescent protein (GFP) marker was used to determine transfection efficiency (Supplementary Fig. S1).

EC6A and EC7A are two mutated Epi-iPSC clones that were obtained by the transfection of normal Epi-iPSCs with *TP53*-targeting and *SMARCB1*-targeting plasmids. These dual knockout cells did not show major morphological differences from normal Epi-iPSCs (Fig. 2A). We also amplified *TP53* and *SMARCB1* target regions in these knockout cells. The theoretical length of *TP53 and SMARCB1* amplicons are 604 bp and 341 bp, respectively. Gel electrophoresis results indicated desired PCR products for both genes, negating on-target plasmid DNA insertional defects (Fig. 2B). SMARCB1 immunostaining demonstrated loss of nuclear expression of the protein in the dual knockout EC6A and EC7A cells, as in CHLA-02-ATRT and CHLA-05-ATRT brain rhabdoid tumor cell lines. (Fig. 2C).

Priorly, transfecting Epi-iPSCs with only *SMARCB1*-targeting plasmid led to poor cell survival. Therefore, the Epi-iPSCs were treated with the *TP53*-targeting plasmid before knocking out *SMARCB1* to increase cell survival. Mutated Epi-iPSC clones EC6 and EC7 were obtained first by transfecting normal Epi-iPSCs with plasmids targeting *TP53*. After 5 passages, the cells did not show signs of cellular death. *TP53* sequencing for both EC6 and EC7 showed an addition of an adenosine nucleotide to exon 4 to generate a premature stop codon in place of Tyr163 (Fig. 3A and B). Both EC6 and EC7 were then subjected to *SMARCB1*-targeting plasmid transfection and renamed EC6A and EC7A. Mutated SMARCB1 in these clones had a deletion of 9 nucleotides in exon 2 that affected three contiguous codons for the amino acids Met38-Phe39-Arg40 (Fig. 4A(i), Fig. 4A(ii), and Fig. 4B). These residues form a loop connecting two alpha helices in the N-terminal domain of the protein (Fig. 4C).

EC6A and EC7A dual knockout Epi-iPSCs underwent germ layer differentiation for pluripotency assessment (Fig. 5A). Upon differentiation into germ layer lineages, the cells were tested for germ layer-specific markers. Both clones expressed CD34, CD43, and VEGFR-2 upon mesoderm differentiation, Pax-6 and Nestin upon ectoderm differentiation, and HNF–3B upon endoderm differentiation (Fig. 5B). The results indicate that the dual knockout Epi-iPSCs retained their capacity to differentiate into any germ layer lineages.

Since early NPCs are the most probable cellular origin of ATRT, EC6A and EC7A cells were briefly induced for neural differentiation to obtain an ATRT-like model (Fig. 6A). The knockout spheroids showed similar morphology to neural progenitor spheroids derived from normal Epi-iPSCs (Fig. 6B). The diameter of EC6A- and EC7A-derived spheroids was mostly in the range of 50–100 μm (Fig. 6C). Calcium signaling assay was performed for normal Epi-iPSC-, EC6A-, and EC7A-derived spheroid cells to monitor their neuronal differentiation [32,33]. Intracellular calcium transients were observed for all cell types (Fig. 7).

3.2. Dual knockout spheroids expressed ATRT biomarkers

RT-PCR was performed to investigate SHH and β-catenin pathways, embryonic, neuronal, and putative ATRT biomarkers in the knockout spheroids (Table 1). EC6A- and EC7A-derived spheroids (EC6A-SP and EC7A-SP onwards) had higher gene expression for all the markers except for *ENO2* (0.8 and 0.5 folds, respectively) when compared with normal Epi-iPSC-derived spheroid (Epi-iPSC-SP, control) (Fig. 8). Genes that showed at least three-fold higher expression than the control for both EC6A-SP and EC7A-SP were - *GLI1* (6.5 and 4.5 folds, respectively) (Fig. 8A), *OCT4* (5.5 and 20.6 folds, respectively), *NANOG* (4.0 and 14 folds, respectively) (Fig. 8B), and *OPN* (4 and 3.2, respectively) (Fig. 8D); *STAT3* was highly expressed in EC6A- and EC7A-derived spheroid cells (3 and 1.9 folds, respectively) (Fig. 8D). The low expression of *ENO2* is shown in Fig. 8C. A summary of RT-PCR results can be found in Table 2.

In addition to mRNA expression analysis, we performed immunocytochemistry (ICC) to examine protein expression of normal Epi-iPSC-, EC6A-, and EC7A-derived spheroid cells with two ATRT cell lines as control groups. Osteopontin, β-catenin, Pax-6, Ki-67, Nestin, Oct-4, NANOG, GLI1, GLI2, and Nucleophosmin (NPM) were the markers of interest in the ICC experiment (Fig. 9). Ki-67 and Nestin expression was

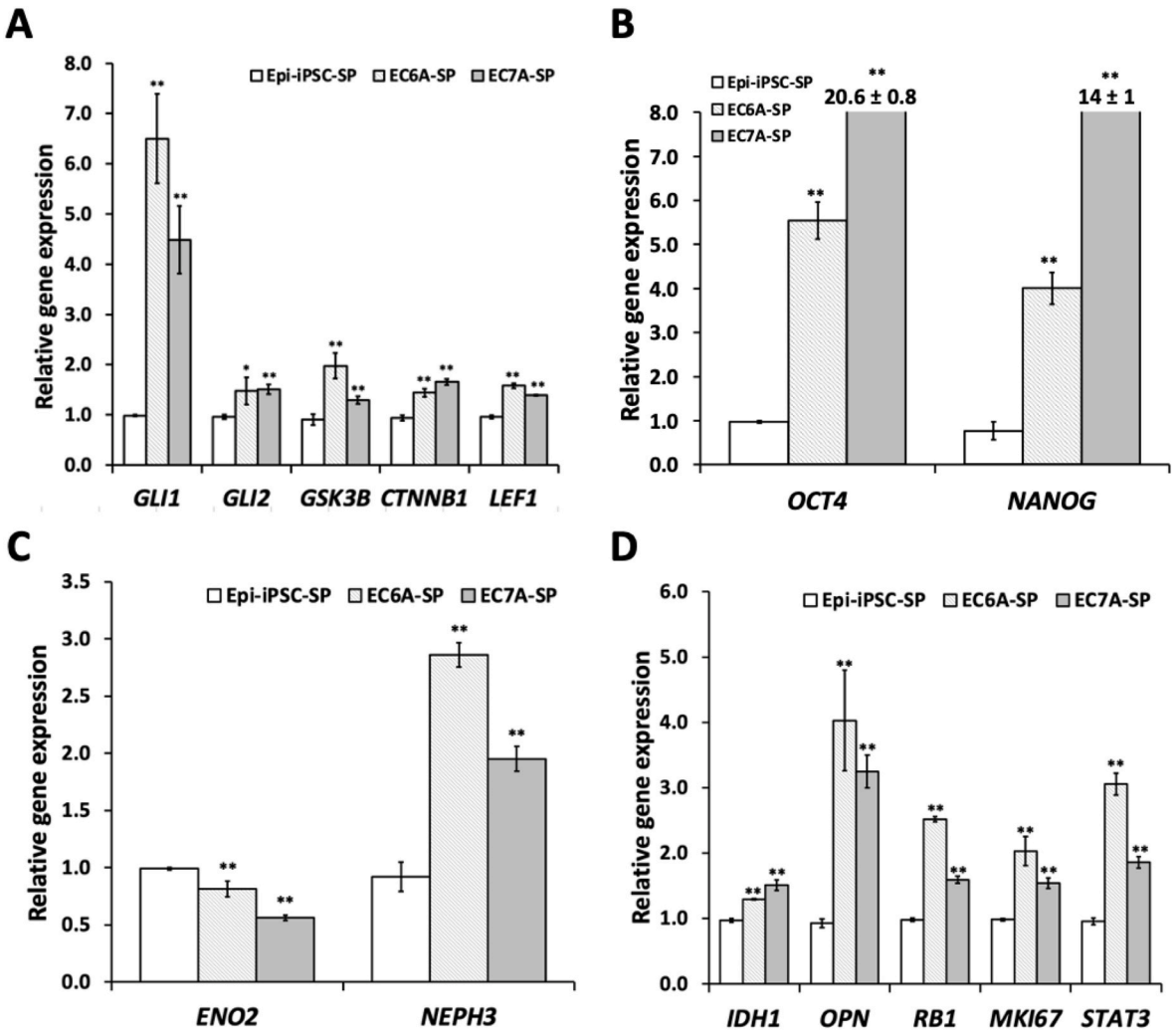

Fig. 8. Characterization of the ATRT-like model with RT-PCR. Normal Epi-iPSC and both the knockout clones (EC6A and EC7A) were subjected to neural induction. The spheroids were harvested post-induction and characterized for **(A)** SHH and β-catenin pathways, **(B)** embryonic, **(C)** neuronal, and **(D)** potential ATRT biomarkers. *: *p*-value <0.05 when compared with the control, Epi-iPSC-SP; **: *p*-value <0.01 when compared with the control, Epi-iPSC-SP. Epi-iPSC-SP: normal Epi-iPSC-derived spheroids; EC6A-SP: EC6A-derived ATRT-like spheroids; EC7A-SP: EC7A-derived ATRT-like spheroids; *GLI1*: glioma-associated oncogene family zinc finger 1; *GLI2*: glioma-associated oncogene family zinc finger 2; *GSK3B*: glycogen synthase kinase 3 beta; *CTNNB1*: catenin beta-1; *LEF1*: lymphoid enhancer-binding factor 1; *OCT4*: octamer-binding protein 4; *NANOG*: Nanog homeobox; *ENO2*: enolase 2; *NEPH3*: kirre-like nephrin family adhesion molecule 2; *IDH1*: isocitrate dehydrogenase NADP(+) 1; *OPN*: osteopontin; *RB1*: retinoblastoma transcriptional corepressor 1; *MKI67*: marker of proliferation Ki-67; *STAT3*: signal transducer and activator of transcription 3.

Table 2
Summary of RT-PCR results for normal Epi-iPSC- vs dual knockout Epi-iPSC-derived spheroids.

Marker type	Gene	EC6A-SP vs EpiPSC-SP	EC7A-SP vs EpiPSC-SP
SHH pathway	*GLI1*	Increased	Increased
	GLI2	Increased	Increased
β-catenin pathway	*GSK3B*	Increased	Increased
	CTNNB1	Increased	Increased
	LEF1	Increased	Increased
Embryonic	*OCT4*	Increased	Increased
	NANOG	Increased	Increased
Neuronal	*ENO2*	Decreased	Decreased
	NEPH3	Increased	Increased
Potential ATRT biomarkers	*IDH1*	Increased	Increased
	OPN	Increased	Increased
	RB1	Increased	Increased
	MKI67	Increased	Increased
	STAT3	Increased	Increased

observed across all groups, indicating proliferative capacity and neural characteristics of the cells. β-catenin expression was lower only in Epi-iPSC-SP, implying its higher activity in SMARCB1-deficient cells. Pronounced expression of both Oct-4 and NANOG in EC6A-SP and EC7A-SP was comparable to that in two ATRT cell lines, endorsing the embryonal nature of ATRT and knockout spheroids. GLI1 protein expression was lower in Epi-iPSC-SP, EC6A-SP, and EC7A-SP when compared to the ATRT cell lines. Interestingly, GLI2, NPM, and Osteopontin proteins were expressed by all cells, which are putative ATRT biomarkers [34,35]. Finally, Pax-6 expression was higher in ATRT cell lines and EC7A-SP but lower in Epi-iPSC-SP and EC6A-SP (Fig. 9).

3.3. Drug treatment decreased the viability of ATRT-like cells

The effect of enzyme inhibitors and a channel blocker on the EC6A-SP and EC7A-SP cell viability was tested (Fig. 10A and B). The spheroids were harvested, dissociated, and replated on a *Matrigel*™-coated surface before being treated with ribociclib, PTC-209, or the combination of clofilium tosylate and pazopanib. MTT assay was used to determine the

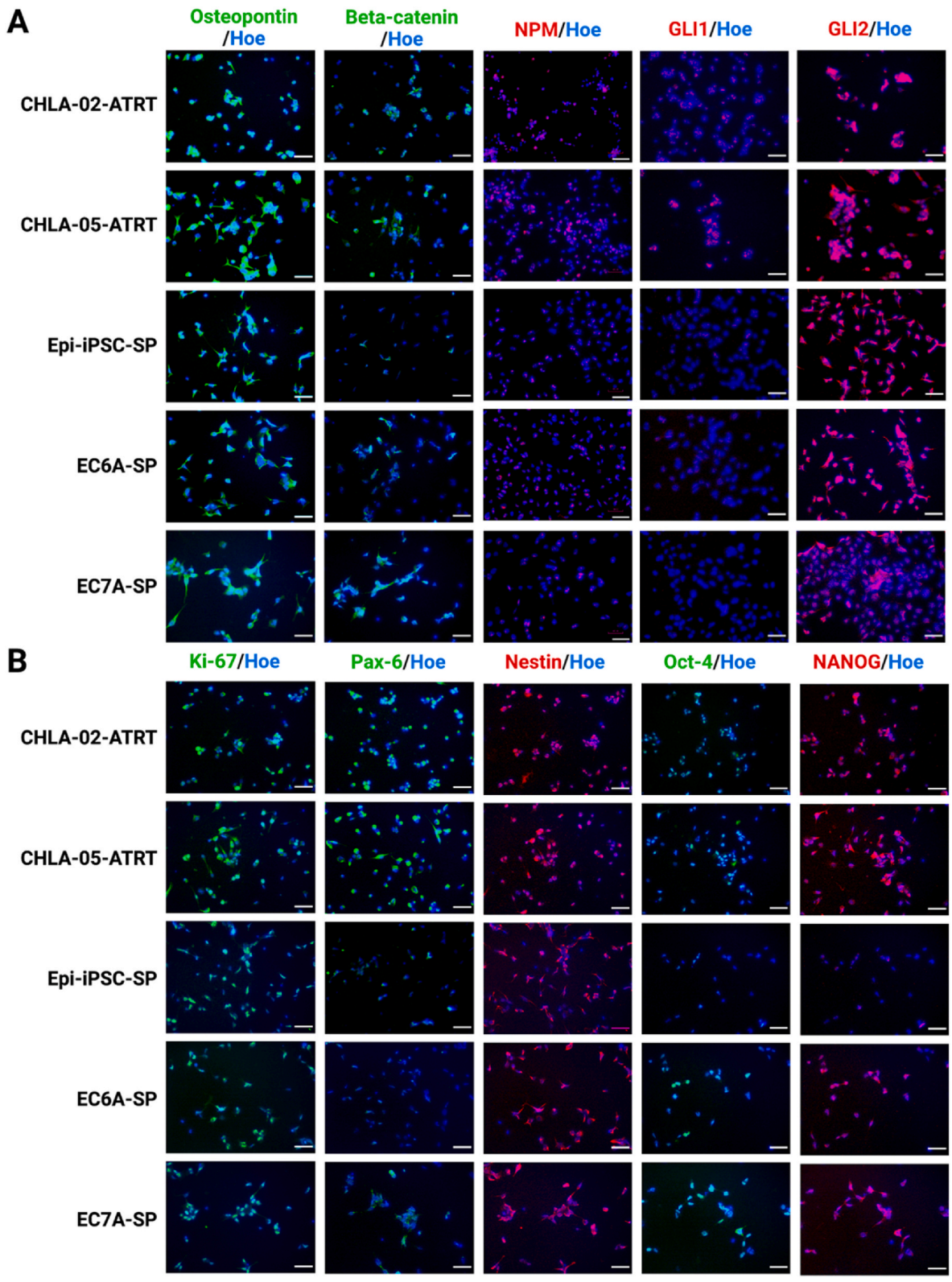

Fig. 9. Immunocytochemistry images for ATRT biomarker detection. ICC was performed for ATRT cell lines CHLA-02-ATRT and CHLA-05-ATRT, normal Epi-iPSC-derived spheroid cells, and EC6A- and EC7A-derived spheroid cells. Separate ICC images for each marker can be found in Supplementary Fig. S6. NPM: nucleophosmin; GLI1: zinc finger protein GLI1; GLI2: zinc finger protein GLI2; Ki-67: proliferation marker protein Ki-67; Pax-6: paired box protein Pax-6; Oct-4: octamer-binding transcription factor 4; NANOG: homeobox protein NANOG; Hoe: Hoechst 33342. **Scale bar: 50 μm.**

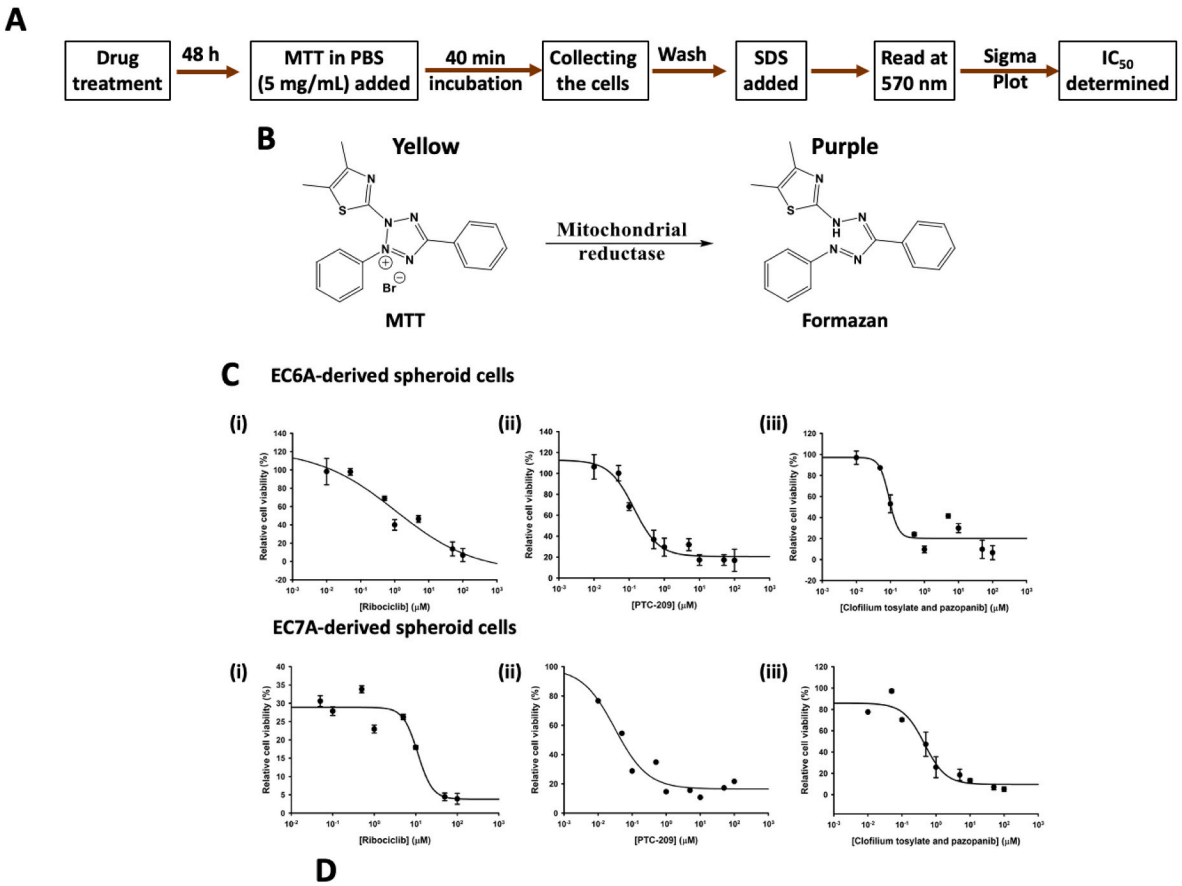

Drug treatments		IC_{50} (μM)	Hillslope
EC6A-SP	RB	1.1 ± 1.1	−0.4 ± 0.3
	PTC	0.14 ± 0.03	−1.2 ± 0.3
	CT+PZ	0.09 ± 0.01	−3.1 ± 1.5
EC7A-SP	RB	11.2 ± 1.9	−2.5 ± 1.1
	PTC	0.03 ± 0.03	−0.9 ± 0.4
	CT+PZ	0.046 ± 0.09	−1.4 ± 0.4

Fig. 10. Determining the IC_{50} values for drug treatments of the ATRT-like model (A) The drug treatment scheme for EC6A- and EC7A-derived ATRT-like spheroids. The spheroids were collected, dissociated, and replated into wells of a 96-well plate to test the drug effect 48 h after the treatment. **(B)** Reduction of MTT inside live cells to elicit a color change. **(C)** IC_{50} curves for different drug treatments of EC6A- and EC7A-derived spheroids: **(i)** ribociclib, **(ii)** PTC-209, and **(iii)** the combination of clofilium tosylate and pazopanib. **(D)** The reported IC_{50} values and hillslope values. SB431542: SMAD protein inhibitor; Y-27632: rho-associated protein kinase inhibitor; FGF2: fibroblast growth factor 2; MTT: 3-(4,5-dimethylthiazol-2-yl)-2,5-diphenyl tetrazolium bromide; PBS: phosphate-buffered saline; SDS: sodium dodecyl sulfate; IC_{50}: half-maximal inhibitory concentration; RB: ribociclib; PTC: PTC-209; CT + PZ: the combination of clofilium tosylate and pazopanib.

IC_{50} and the hillslope values (Fig. 10C and D). The combination of clofilium tosylate and pazopanib was chosen because the combination induced the lowest IC_{50} values in ATRT cell lines CHLA-02-ATRT and CHLA-05-ATRT compared with each drug alone (Supplementary Fig. S2) [36]. Both PTC-209 and the combination of clofilium tosylate and pazopanib induced the lowest IC_{50} in both EC6A-SP (0.14 and 0.03 μM, respectively) and EC7A-SP (0.09 and 0.046 μM, respectively) (Fig. 10D).

4. Discussion

ATRT is a highly malignant embryonal tumor that comprises immature, large tumor cells of mixed histopathology and commonly affects children younger than age 3 [37]. A spectrum of inactivating mutations in both alleles of a single tumor suppressor gene, *SMARCB1*, is primarily attributable to ATRT formation [38]. The remarkable genomic simplicity of the rare tumor was leveraged to model ATRT-like spheroids from human episomal iPSCs in this study to improve the scalability of the disease platform and throughput of drug evaluation.

We used CRISPR/Cas9 gene editing technology and generated premature termination mutation in *TP53* and deletion mutation in *SMARCB1* (Figs. 3 and 4). SMARCB1 amino acids Met38-Phe39-Arg40 deleted in this study form a loop that connects two alpha helices of the DNA-binding region (Fig. 4). Arg40 acts as the key residue that inserts its side chain into the DNA major groove for binding [31]. In addition, Lys45 on the downstream alpha helix acts as one of the primary amino acids facilitating DNA binding [31]. Arg40 and Lys45 are highly conserved across the metazoan *SMARCB1* genes [31]. Genomic analyses of ATRT have reported nonsense (c.118C > T) and frameshift (c.118del) mutations impacting the critical Arg40 residue of SMARCB1 in patients [39,40]. Additionally, the mutations of these three amino acids have been found in cancers of different tissue origins, such as breast, stomach, intestine, and liver (Supplementary Fig. S3). In this

study, the deletion of these residues proved sufficient to diminish the nuclear expression of the SMARCB1 protein in the knockout cells (Fig. 2). Moreover, the TP53 nonsense mutation (p.Tyr163*) effected here has been found in glioma (Supplementary Fig. S4). The truncated TP53 only retained 162 out of 393 amino acids (~41%).

The *TP53*-knockout cell lines did not commit apoptosis or show any signs of cell death after transfection with *SMARCB1*-targeting CRISPR/Cas9 plasmid. Dual knockout Epi-iPSCs could also successfully differentiate into any germ layer lineages upon appropriate induction (Fig. 5 and Supplementary Fig. S5). The transfection procedure is reproducible since both EC6A and EC7A clones had the same *SMARCB1* and *TP53* mutations. Therefore, neurally induced EC6A and EC7A can be treated as comparable ATRT-like models.

The model was derived from Epi-iPSC, which virtually has no footprints and is free of all reprogramming genes and mutations. Although deriving an ATRT model from differentiated dual knockout (*SMARCB1*$^{-/-}$ and *TP53*$^{-/-}$) iPSCs has been reported previously [2], the procedure requires injecting the cells into the mouse brain. The approach used in this study did not require animals but the early-stage cerebellum differentiation protocol to generate spheroids [41]. The model's gene expression profile showed high similarity with that of patient-derived ATRT cell lines, including upregulated SHH and β-catenin pathway [4], higher expression of *OCT4* and *NANOG* embryonic markers [42], higher *OPN* [34], as well as a lower level of specific neuronal marker *ENO2* (Fig. 8). *NEPH3* is a cerebellar-specific Purkinje cell progenitor marker that has been used in characterizing iPSC-derived cerebellar spheroids [28,41] and is overexpressed by the ATRT-like model. High expression of *NEPH3* and low level of *ENO2* transcript post-differentiation suggests that the model had an undifferentiated phenotype similar to real ATRT tumors. In addition, higher *MKI67* and *STAT3* expression further promote cell proliferation and the oncogenic phenotype of the model [11]. Immunocytochemistry confirmed an activated β-catenin pathway in the knockout spheroids, though the overshoot of *GLI1* mRNA expression did not translate into an increased protein expression of the SHH pathway component (Fig. 9). Higher Oct-4 and NANOG protein expression was observed in the knockout spheroids to endorse the desirable embryonal property of ATRT in the established model (Fig. 9). Other ATRT biomarkers such as GLI2, NPM, and Osteopontin were also expressed by the knockout spheroids (Fig. 9) [34,35,42]. Taken together, the gene and protein expression profiles imply that EC6A- and EC7A-derived spheroids may serve as an ATRT-like model.

The majority of ATRT do not carry any mutations in the *TP53* gene [40,41,43]. However, attempts to knock out *SMARCB1* alone in hiPSCs only resulted in cellular death. Even using a mouse model, homozygous deletion of SMARCB1 in Nestin-positive progenitor led to cell death that could not be rescued by *TP53* ablation [44]. In addition, the inactivation of both TP53 and SMARCB1 resulted in malignant tumors in the cerebellum [44]. Therefore, inactivating the function of both TP53 and SMARCB1 before neural induction could be critical for generating an ATRT model. Indeed, ATRT cell lines express TP53 as a tumor suppressor marker. However, the function of TP53 is regulated by the oncogenes MDM2 and MDM4 [45]. MDM2 marks TP53 for proteasomal degradation, and MDM4 binds to TP53 to inhibit TP53 transcription function [46]. Inhibiting MDM2 or both MDM2 and MDM4 using idasanutlin or ATSP-7041 could make ATRT cells vulnerable to the TP53-mediated apoptosis pathway [45]. On the other hand, idasanutlin or ATSP-7041 did not demonstrate a similar effect on other TP53 wild-type cancer cell lines [45]. Therefore, abolishing the TP53 function before SMARCB1's could be a prerequisite in generating the ATRT model. The model can still be improved in the future, bypassing the need for *TP53* mutation in NPCs to recapitulate the ATRT genotype and phenotype more accurately.

We further tested the effects of some small-molecule drugs on our ATRT-like model (Fig. 10). Clofilium tosylate, a potassium channel blocker, has been shown to perturb protein metabolism and, in concert with pazopanib, induce apoptosis of rhabdoid tumor (RT) cells *in vitro* [36]. Pazopanib acts as a dual inhibitor of platelet-derived growth factor receptor (PDGFR) and fibroblast growth factor receptor 2 (FGFR2) on the membrane, both of which are co-activated in RT [13]. Ribociclib is an inhibitor of CDK4/6, two cell cycle regulatory proteins that are dysregulated in SMARCB1-deficient cells [13]. Ribociclib demonstrates acceptable safety and could be a potential treatment for RT patients [47]. Finally, PTC-209 inhibits a major component of the Polycomb complex protein BMI-1, which functions antagonistically to SMARCB1 [48]. Hillslope values for all drug treatments of the ATRT-like model were negative, demonstrating a decrease in cell viability as drug concentration increased. In addition, clofilium tosylate treatment had a higher effect on the ATRT cells than pazopanib, and the combination of the two drugs had the lowest IC_{50} values. The latter finding is consistent with the literature which demonstrates clofilium tosylate and pazopanib combination is highly effective against ATRT models [36]. This work shows that PTC-209 is potent against a rhabdoid-like model, which has already shown high potency against other types of cancer [49]. A systematic study of drug effects on ATRT markers in the established model may provide a comprehensive understanding of molecular phenomena upon drug treatment and therefore is a future research direction.

The knockout iPSC-derived ATRT-like model provides a reproducible and scalable human *in vitro* platform for a plethora of applications. The establishment of the tumor model by inactivating the tumor suppressor genes signifies that patient-derived iPSCs harboring individual-specific driver mutations can be a promising tool for personalized cancer modeling. The strategy improves the scalability of the patient-specific tumor platforms and provides a consistent, streamlined approach to disease modeling. The provided scheme also offers the scope for studying molecular events in tumor initiation, identification of aberrant pathways and drug targets, and semi-high-throughput therapeutic evaluation for clinical decision-making. However, the tumor-forming ability and invasion capacity of the established model remains to be investigated, which might be tested *in vivo* for further characterization of the model. Moreover, our model lacks native tumor complexity such as vasculature and microenvironment that modulate tumor invasion, metastasis, and drug response in patients and animal models. Despite the limitations, our ATRT-like model is an attractive *in vitro* tumor platform that minimizes the need for primary tumor tissues or xenograft animal models addressing the issues of patient sample availability and human relevance, respectively.

5. Conclusions

We report the generation of an ATRT-like model from human episomal iPSCs by introducing deletion and nonsense mutations into *SMARCB1* and *TP53* tumor suppressor genes, respectively. Dual knockout Epi-iPSCs retained pluripotency and underwent neural induction to form ATRT-like spheroids. The knockout spheroids overexpressed canonical Wnt pathway genes and embryonic biomarkers and exhibited undifferentiated phenotype via upregulated stem cell markers *OCT4* and *NANOG* and downregulated neuronal marker ENO2. The model also expressed cerebellar-specific Purkinje cell progenitor marker *NEPH3* and cancer biomarkers Nucleophosmin, Osteopontin, and Ki-67. Finally, Ribociclib, PTC-209, and the combination of clofilium tosylate and pazopanib decreased the cell viability of the ATRT-like cells. The reported modeling scheme might be useful for deriving personalized tumor models with patient-specific mutations and drug testing.

Funding

This project was supported mainly by the Florida Department of Health (FDOH) Live Like Bella awards (9LA01 and 21L10 to Q.-X.S. and Y.L.), an FSU Council on Research & Creativity (CRC) planning grant, the Pfeiffer Professorship for Cancer Research in Chemistry and Biochemistry from the College of Arts & Sciences, and an Endowed Chair

Professorship in Cancer Research from anonymous donors (to Q.-X.S.). This work was partially supported by the National Science Foundation (CBET-1652992 and CBET-1917618 to Y.L.).

Institutional review board statement

Not Applicable.

Informed consent statement

Not applicable.

Data availability statement

The datasets generated and used/or analyzed are published in this paper and Supplementary Information, and available from the corresponding author upon request.

Ethics approval and consent to participate

Not applicable.

CRediT authorship contribution statement

Timothy Hua: Conceptualization, Data curation, Formal analysis, Investigation, Methodology, Visualization, Writing – original draft, Writing – review & editing. **Yu Xue:** Data curation, Formal analysis, Investigation, Methodology, Validation, Visualization, Writing – review & editing. **Drishty B. Sarker:** Data curation, Formal analysis, Investigation, Methodology, Validation, Visualization, Writing – original draft, Writing – review & editing. **Sonia Kiran:** Data curation, Formal analysis, Investigation, Methodology, Validation, Visualization, Writing – review & editing. **Yan Li:** Formal analysis, Funding acquisition, Methodology, Project administration, Resources, Supervision, Writing – review & editing. **Qing-Xiang Amy Sang:** Conceptualization, Formal analysis, Funding acquisition, Investigation, Methodology, Project administration, Resources, Supervision, Validation, Visualization, Writing – original draft, Writing – review & editing.

Declaration of competing interest

None.

Acknowledgments

The authors would like to thank Florida State University (FSU) Research Facilities, Brian K. Washburn, Diego Zorio, and Kristina Poduch for their assistance with RT-PCR experiments at the Molecular Cloning Facility at the Department of Biological Sciences, and Beth Alexander and Ruth Didier for their cooperation with flow cytometry analysis at the FSU Flow Cytometry Laboratory at the College of Medicine. We would also like to thank Jesse Tuner for his advice on the transfection experiment and his help with sequencing. The graphical abstract was created with Biorender.com.

Appendix A. Supplementary data

Supplementary data to this article can be found online at https://doi.org/10.1016/j.bioactmat.2023.08.009.

References

[1] R.A. Ramli, et al., Identification of the cellular origin and" stemness" phenotype of Malignant Rhabdoid Tumors (MRT) may represent a new therapeutic approach in paediatric oncology, Cancer Res. 77 (2017), 4875-4875.
[2] Y. Terada, et al., Human pluripotent stem cell-derived tumor model uncovers the embryonic stem cell signature as a key driver in atypical teratoid/rhabdoid tumor, Cell Rep. 26 (2019) 2608–2621, e2606.
[3] K.H. Kim, C.W. Roberts, Mechanisms by which SMARCB1 loss drives rhabdoid tumor growth, Cancer Genet. 207 (2014) 365–372.
[4] K. Kohashi, Y. Oda, Oncogenic roles of SMARCB1/INI1 and its deficient tumors, Cancer Sci. 108 (2017) 547–552.
[5] L.B. Rorke, R.J. Packer, J.A. Biegel, Central nervous system atypical teratoid/rhabdoid tumors of infancy and childhood: definition of an entity, J. Neurosurg. 85 (1996) 56–65.
[6] N.C. Institute, Atypical teratoid rhabdoid tumor (ATRT) diagnosis and treatment. https://www.cancer.gov/rare-brain-spine-tumor/tumors/atrt.
[7] U.H. Athale, J. Duckworth, I. Odame, R. Barr, Childhood atypical teratoid rhabdoid tumor of the central nervous system: a meta-analysis of observational studies, J. Pediatr. Hematol./oncol. 31 (2009) 651–663.
[8] K.F. Ginn, A. Gajjar, Atypical teratoid rhabdoid tumor: current therapy and future directions, Front. Oncol. 2 (2012) 114.
[9] C.S. Lau, K. Mahendraraj, R.S. Chamberlain, Atypical teratoid rhabdoid tumors: a population-based clinical outcomes study involving 174 patients from the Surveillance, Epidemiology, and End Results database (1973–2010), Cancer Manag. Res. (2015) 301–309.
[10] E.A. Richardson, B. Ho, A. Huang, Atypical teratoid rhabdoid tumour: from tumours to therapies, J. Korean Neurosurg. Soc. 61 (2018) 302–311.
[11] W.-H. Liu, et al., Cisplatin-selected resistance is associated with increased motility and stem-like properties via activation of STAT3/Snail axis in atypical teratoid/rhabdoid tumor cells, Oncotarget 6 (2015) 1750–1768.
[12] I. Slavc, et al., Atypical teratoid rhabdoid tumor: improved long-term survival with an intensive multimodal therapy and delayed radiotherapy. The Medical University of Vienna Experience 1992–2012, Cancer Med. 3 (2014) 91–100.
[13] G.W. Cooper, A.L. Hong, SMARCB1-deficient cancers: novel molecular insights and therapeutic vulnerabilities, Cancers 14 (2022) 3645.
[14] E.L. Mora-Blanco, et al., Activation of β-catenin/TCF targets following loss of the tumor suppressor SNF5, Oncogene 33 (2014) 933–938.
[15] Z. Jagani, et al., Loss of the tumor suppressor Snf5 leads to aberrant activation of the Hedgehog-Gli pathway, Nat. Med. 16 (2010) 1429–1433.
[16] I. Versteege, S. Medjkane, D. Rouillard, O. Delattre, A key role of the hSNF5/INI1 tumour suppressor in the control of the G1-S transition of the cell cycle, Oncogene 21 (2002) 6403–6412.
[17] J.W. Harbour, R.X. Luo, A. Dei Santi, A.A. Postigo, D.C. Dean, Cdk phosphorylation triggers sequential intramolecular interactions that progressively block Rb functions as cells move through G1, Cell 98 (1999) 859–869.
[18] O. Stevaux, N.J. Dyson, A revised picture of the E2F transcriptional network and RB function, Curr. Opin. Cell Biol. 14 (2002) 684–691.
[19] B.L. Betz, M.W. Strobeck, D.N. Reisman, E.S. Knudsen, B.E. Weissman, Re-expression of hSNF5/INI1/BAF47 in pediatric tumor cells leads to G1arrest associated with induction of p16ink4a and activation of RB, Oncogene 21 (2002) 5193–5203.
[20] E. Di Lullo, A.R. Kriegstein, The use of brain organoids to investigate neural development and disease, Nat. Rev. Neurosci. 18 (2017) 573–584.
[21] R. Passier, V. Orlova, C. Mummery, Complex tissue and disease modeling using hiPSCs, Cell Stem Cell 18 (2016) 309–321.
[22] J.A. Thomson, et al., Embryonic stem cell lines derived from human blastocysts, Science 282 (1998) 1145–1147.
[23] M. Eiraku, et al., Self-organizing optic-cup morphogenesis in three-dimensional culture, Nature 472 (2011) 51–56.
[24] M.A. Lancaster, J.A. Knoblich, Organogenesis in a dish: modeling development and disease using organoid technologies, Science 345 (2014), 1247125.
[25] X. Yin, et al., Stem cell organoid engineering, Cell Stem Cell 18 (2016) 25.
[26] Z.I. Khamis, et al., Modeling human brain tumors and the microenvironment using induced pluripotent stem cells, Cancers 15 (2023) 1253.
[27] S. Bian, et al., Genetically engineered cerebral organoids model brain tumor formation, Nat. Methods 15 (2018) 631–639.
[28] K. Muguruma, A. Nishiyama, H. Kawakami, K. Hashimoto, Y. Sasai, Self-organization of polarized cerebellar tissue in 3D culture of human pluripotent stem cells, Cell Rep. 10 (2015) 537–550.
[29] M. Löhle, et al., Differentiation efficiency of induced pluripotent stem cells depends on the number of reprogramming factors, Stem Cell. 30 (2012) 570–579.
[30] N. Rivlin, R. Brosh, M. Oren, V. Rotter, Mutations in the p53 tumor suppressor gene: important milestones at the various steps of tumorigenesis, Genes Cancer 2 (2011) 466–474.
[31] M.D. Allen, S.M. Freund, G. Zinzalla, M. Bycroft, The SWI/SNF subunit INI1 contains an N-terminal winged helix DNA binding domain that is a target for mutations in schwannomatosis, Structure 23 (2015) 1344–1349.
[32] C. Leclerc, I. Néant, M. Moreau, The calcium: an early signal that initiates the formation of the nervous system during embryogenesis, Front. Mol. Neurosci. 5 (2012) 3.
[33] P.J. Morgan, R. Hübner, A. Rolfs, M.J. Frech, Spontaneous calcium transients in human neural progenitor cells mediated by transient receptor potential channels, Stem Cell. Dev. 22 (2013) 2477–2486.
[34] T. Hua, et al., Human malignant rhabdoid tumor antigens as biomarkers and potential therapeutic targets, Cancers 14 (2022) 3685.
[35] P.D. Johann, et al., Atypical teratoid/rhabdoid tumors are comprised of three epigenetic subgroups with distinct enhancer landscapes, Cancer Cell 29 (2016) 379–393.

[36] C. Chauvin, et al., High-throughput drug screening identifies pazopanib and clofilium tosylate as promising treatments for malignant rhabdoid tumors, Cell Rep. 21 (2017) 1737–1745.
[37] M. Severino, et al., Congenital tumors of the central nervous system, Neuroradiology 52 (2010) 531–548.
[38] B. Ho, et al., Molecular subgrouping of atypical teratoid/rhabdoid tumors—a reinvestigation and current consensus, Neuro Oncol. 22 (2020) 613–624.
[39] M. Hasselblatt, et al., High-resolution genomic analysis suggests the absence of recurrent genomic alterations other than SMARCB1 aberrations in atypical teratoid/rhabdoid tumors, Gene Chromosome Cancer 52 (2013) 185–190.
[40] R.S. Lee, et al., A remarkably simple genome underlies highly malignant pediatric rhabdoid cancers, J. Clin. Invest. 122 (2012) 2983–2988.
[41] T. Hua, et al., Cerebellar differentiation from human stem cells through Retinoid, Wnt, and sonic hedgehog pathways, Tissue Eng. 27 (2021) 881–893.
[42] H.-I. Ma, et al., Differential expression profiling between atypical teratoid/rhabdoid and medulloblastoma tumor in vitro and in vivo using microarray analysis, Child's Nerv. Syst. 26 (2010) 293–303.
[43] M.W. Kieran, et al., Absence of oncogenic canonical pathway mutations in aggressive pediatric rhabdoid tumors, Pediatr. Blood Cancer 59 (2012) 1155–1157.
[44] J.M. Ng, et al., Generation of a mouse model of atypical teratoid/rhabdoid tumor of the central nervous system through combined deletion of Snf5 and p53, Cancer Res. 75 (2015) 4629–4639.
[45] T.P. Howard, et al., MDM2 and MDM4 are therapeutic vulnerabilities in malignant rhabdoid TumorsMDM2 and MDM4 are vulnerabilities in rhabdoid tumors, Cancer Res. 79 (2019) 2404–2414.
[46] M. Wade, Y.-C. Li, G.M. Wahl, MDM2, MDMX and p53 in oncogenesis and cancer therapy, Nat. Rev. Cancer 13 (2013) 83–96.
[47] B. Geoerger, et al., A phase I study of the CDK4/6 inhibitor ribociclib (LEE011) in pediatric patients with malignant rhabdoid tumors, neuroblastoma, and other solid tumors, Clin. Cancer Res. 23 (2017) 2433–2441.
[48] S.K. Kia, M.M. Gorski, S. Giannakopoulos, C.P. Verrijzer, SWI/SNF mediates polycomb eviction and epigenetic reprogramming of the INK4b-ARF-INK4a locus, Mol. Cell Biol. 28 (2008) 3457–3464.
[49] S. Vaishnave, BMI1 and PTEN are key determinants of breast cancer therapy: a plausible therapeutic target in breast cancer, Gene 678 (2018) 302–311.